

Nontopological first-order vortices in a gauged $CP(2)$ theory endowed with the Chern-Simons action

R. Casana¹, M. L. Dias¹ and E. da Hora².

¹*Departamento de Física, Universidade Federal do Maranhão,
65080-805, São Luís, Maranhão, Brazil.*

²*Coordenadoria Interdisciplinar de Ciência e Tecnologia,
Universidade Federal do Maranhão,
65080-805, São Luís, Maranhão, Brazil.*

We study a gauged $CP(2)$ model with the Chern-Simons term, focusing our attention on those time-independent radially symmetric configurations with nontopological profile. We proceed the minimization of the effective energy in order to introduce the corresponding first-order framework, from which we define a legitimate self-dual scenario. We solve the resulting first-order equations numerically by means of the finite-difference scheme, from which we depict the nontopological solutions. We also identify a special kind of solutions which can be partially described by an analytical treatment.

PACS numbers: 11.10.Kk, 11.10.Lm, 11.27.+d

I. INTRODUCTION

In the context of classical field models, vortices are those time-independent radially symmetric solutions arising from a planar gauged theory in the presence of a symmetry breaking potential describing the scalar-matter self-interaction [1]. However, due to the high nonlinearity inherent to the symmetry breaking potentials, the corresponding Euler-Lagrange equations of motion can be quite hard to solve (even numerically).

On the other hand, under very special circumstances, time-independent vortices can also be obtained by solving a particular set of coupled first-order differential equations (instead of the second-order Euler-Lagrange ones), these equations being usually obtained via the minimization of the effective energy, the resulting solutions saturating a well-defined lower bound for the energy itself [2].

In this sense, first-order vortices were firstly obtained in the context of the Maxwell-Higgs electrodynamics in which the corresponding vacuum manifold exhibits asymmetric states only (the resulting vortices presenting the typical topological behavior) [3]. In addition, first-order vortices were verified to occur also in the Chern-Simons-Higgs theory, with the vacuum structure presenting now both symmetric and asymmetric states (the corresponding configurations being topological or nontopological, respectively) [4].

Furthermore, legitimate vortex solutions satisfying first-order differential equations were also investigated in connection to the noncanonical gauge theories [5], the resulting structures being applied in the study of some interesting cosmological problems [6].

In such a context, an interesting issue is the search for the first-order vortices inherent to a gauged $CP(N-1)$ model, mainly due to the phenomenological connection between such a theory and the four-dimensional Yang-Mills-Higgs one [7].

In this sense, in a recent work, the time-independent

solutions with radial symmetry arising from a gauged $CP(2)$ model in the presence of the Maxwell's term were studied, the author focusing his attention on how some relevant quantities (such as the total energy and the magnetic field) depend on the parameters defining the model [8]. In that work, however, these configurations were obtained directly from the second-order Euler-Lagrange equations of motion.

In the sequel, some of us have developed a particular first-order framework consistent with the very same theoretical scenario described above. Indeed, we have proceeded the minimization of the resulting energy, from which we have introduced the corresponding first-order equations and a well-defined lower bound for the energy itself, the potential supporting self-duality presenting only asymmetric vacua, which we have used to study time-independent vortices with a topological profile [9].

We have also studied the radially symmetric solitons inherent to a planar $CP(2)$ model endowed by the Maxwell's term multiplied by a nontrivial dielectric function, our main conclusion being that the potential (and the vacuum manifold it defines) supporting self-duality depends on the dielectric function itself [10]. We have then chosen such a function in order to change the original vacuum manifold into a dot surrounded by a circle (the centered dot representing a symmetric vacuum), from which we have obtained nontopological vortices with no electric charge.

Furthermore, we have recently considered a $CP(2)$ theory in the presence of the Chern-Simons term (instead of the Maxwell's one), via which we have verified the existence of first-order vortices with a nonvanishing electric field, the resulting configurations presenting the well-known topological profile [11].

Now, we go a little bit further on the aforementioned investigation by studying those nontopological vortices satisfying the first-order framework consistent with the gauged $CP(2)$ model endowed by the Chern-Simons action.

In order to present our results, this work is organized

as follows: in the next Section II, we introduce the overall model and the conventions inherent to it, focusing our attention on those radially symmetric time-independent configurations. In the Section III, we split our investigation into two different branches based on our choices for an additional profile function which appears in the radially symmetric ansatz. We then proceed the minimization of the effective energy, from which we introduce the corresponding first-order framework (i.e. the first-order equations themselves and a well-defined lower bound for the total energy), the starting-point being a differential constraint whose solution is the particular potential supporting self-duality. In the sequel, we use these expressions in order to define a coherent first-order scenario. We solve the first-order equations numerically by means of the finite-difference scheme, from which we depict the solutions to the relevant fields. We also implement a convenient assumption, from which we get an approximate analytical description of those numerical solutions, therefore explaining in details their main properties. In addition, we identify a second type of numerical solutions that can not be predicted by any analytical treatment. Finally, in the last Section IV, we present our main conclusions and perspectives regarding future investigations.

In what follows, we use $\eta^{\mu\nu} = (+ - -)$ as the metric signature for the flat spacetime, together with the natural units system, for the sake of convenience.

II. THE MODEL

We begin our letter by reviewing the first-order formalism presented in [11], the starting-point being the planar Lagrange density describing the interaction between the electromagnetic field (introduced via the Chern-Simons term) and the complex $CP(N - 1)$ one, i.e. (here, $\epsilon^{012} = +1$)

$$\mathcal{L} = -\frac{\kappa}{4}\epsilon^{\alpha\mu\nu}A_\alpha F_{\mu\nu} + (P_{ab}D_\mu\phi_b)^* P_{ac}D^\mu\phi_c - V(\phi), \quad (1)$$

the $CP(N - 1)$ sector itself being constrained to satisfy $\phi_a^*\phi_a = h$. Here,

$$F_{\mu\nu} = \partial_\mu A_\nu - \partial_\nu A_\mu \quad (2)$$

is the electromagnetic field strength tensor and

$$D_\mu\phi_a = \partial_\mu\phi_a - igA_\mu Q_{ab}\phi_b \quad (3)$$

stands for the usual covariant derivative (in which Q_{ab} is a diagonal real matrix). Also, $P_{ab} = \delta_{ab} - h^{-1}\phi_a\phi_b^*$ is a projection operator.

It is instructive to point out that the theory in (1) is manifestly invariant under the global $SU(N)$ transformation (beyond the usual local $U(1)$ one). In this sense, given that regular solitons are known to occur during a symmetry breaking phase transition, the first-order scenario we study in this work is expected to contain a self-interaction potential depending on only one component

of the original $CP(N - 1)$ scalar sector (therefore giving rise to a spontaneous breaking of the original $SU(N)$ symmetry), see the discussion in the Ref. [11].

The Euler-Lagrange equation for the Abelian gauge field coming from (1) is

$$\frac{\kappa}{2}\epsilon^{\lambda\mu\nu}F_{\mu\nu} = J^\lambda, \quad (4)$$

where

$$J^\lambda = ig \left[P_{ac}D^\lambda\phi_c (P_{ab}Q_{bf}\phi_f)^* - (P_{ab}D^\lambda\phi_b)^* P_{ac}Q_{cb}\phi_c \right], \quad (5)$$

is the current 4-vector.

It follows from the Eq. (4) that the Gauss law for time-independent configurations reads

$$\kappa B = \rho, \quad (6)$$

where $B = F_{21}$ stands for the magnetic field and

$$\rho = g^2 A^0 \left[(P_{ab}Q_{ab}\phi_b)^* P_{ac}Q_{cd}\phi_c - (P_{ab}Q_{ab}\phi_b) (P_{ac}Q_{cd}\phi_c)^* \right], \quad (7)$$

represents the stationary charge density. Here, given that $A^0 = 0$ does not solve (6) identically, we conclude that the time-independent structures arising from (1) are electrically charged. In addition, in view of the Gauss law (6), it is possible to point out that the total magnetic flux is proportional to the total electric charge, and vice-versa.

In what follows, we focus our attention on those time-independent radially symmetric solutions defined by the usual vortex map

$$A_i = -\frac{1}{gr}\epsilon^{ij}n^j A(r), \quad (8)$$

$$\begin{pmatrix} \phi_1 \\ \phi_2 \\ \phi_3 \end{pmatrix} = h^{\frac{1}{2}} \begin{pmatrix} e^{im_1\theta} \sin(\alpha(r)) \cos(\beta(r)) \\ e^{im_2\theta} \sin(\alpha(r)) \sin(\beta(r)) \\ e^{im_3\theta} \cos(\alpha(r)) \end{pmatrix}, \quad (9)$$

where m_1 , m_2 and m_3 are positive integers defining the vorticity of the resulting configurations. Also, ϵ^{ij} is the planar Levi-Civita symbol ($\epsilon^{12} = +1$) and $n^j = (\cos\theta, \sin\theta)$ stands for the unit vector. In this case, the magnetic field can be verified to be given by

$$B(r) = -\frac{1}{gr}\frac{dA}{dr}, \quad (10)$$

being a function of the radial coordinate r only.

Here, we point out that regular solutions presenting no divergences are attained via those profile functions $\alpha(r)$ and $A(r)$ satisfying the conditions

$$\alpha(r \rightarrow 0) \rightarrow 0 \quad \text{and} \quad A(r \rightarrow 0) \rightarrow 0, \quad (11)$$

which will be used later below. Moreover, given that we are interested in those first-order solitons with a nontopological profile, the asymptotic behavior of $\alpha(r)$ and $A(r)$ can be supposed to be such as

$$\alpha(r \rightarrow \infty) \rightarrow 0 \quad \text{and} \quad \frac{dA}{dr}(r \rightarrow \infty) \rightarrow 0, \quad (12)$$

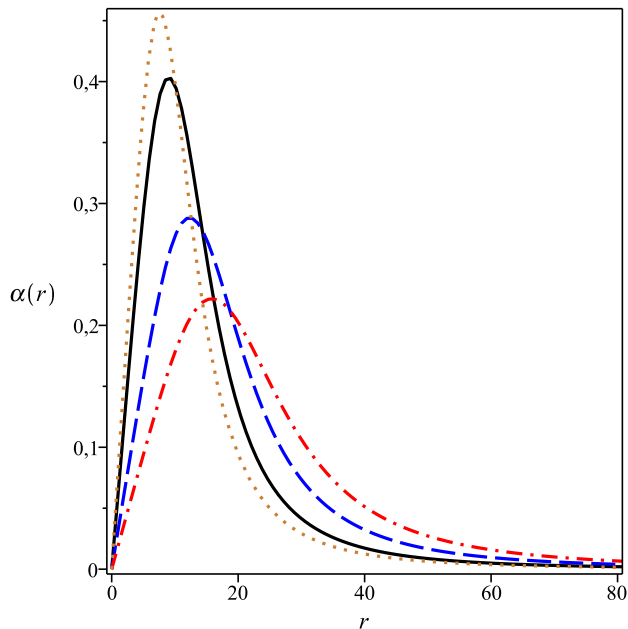


FIG. 1. Numerical solutions to $\alpha(r)$ coming from the first-order equations (32) and (33) in the presence of the boundary conditions (11) and (12). Here, we have chosen $m = h = g = k = 1$ and $r_0 = 10$ (solid black line), $r_0 = 15$ (dashed blue line) and $r_0 = 20$ (dash-dotted red line). We have also plotted the approximate analytical solution (42) for $m = h = g = k = 1$ and $r_0 = 10$ (dotted orange line), for comparison.

with $A_\infty \equiv A(r \rightarrow \infty)$ finite.

Now, it is important to highlight that, regarding the combination between the winding numbers m_1 , m_2 and m_3 and the charge matrix Q_{ab} , there are two different choices supporting the existence of topologically nontrivial configurations (both ones with $m_3 = 0$): (i) $m_1 = -m_2 = m$ and $Q = \lambda_3/2$ (with $\lambda_3 = \text{diag}(1, -1, 0)$), and (ii) $m_1 = m_2 = m$ and $Q = \lambda_8/2$ ($\sqrt{3}\lambda_8 = \text{diag}(1, 1, -2)$). However, it is known that these two scenarios simply mimic each other, being then phenomenologically equivalent. Therefore, in this manuscript, we consider only the first choice, i.e.

$$Q = \frac{1}{2} \text{diag}(1, -1, 0), \quad (13)$$

with $m_1 = -m_2 = m$ and $m_3 = 0$.

In this case, the radially symmetric Euler-Lagrange equation for the additional profile function $\beta(r)$ reads

$$\frac{d^2\beta}{dr^2} + \left(\frac{1}{r} + 2 \cot \alpha \frac{d\alpha}{dr}\right) \frac{d\beta}{dr} = H \sin^2 \alpha \sin(4\beta), \quad (14)$$

where

$$H(r) = \frac{1}{r^2} \left(m - \frac{A}{2}\right)^2 - \frac{g^2 (A_0)^2}{4} \sin^2 \alpha \quad (15)$$

is an auxiliary function, the solutions for $\beta(r)$ being ($k \in \mathbb{Z}$)

$$\beta(r) = \beta_1 = \frac{\pi}{4} + \frac{\pi}{2}k \quad \text{or} \quad \beta(r) = \beta_2 = \frac{\pi}{2}k, \quad (16)$$

this way defining two a priori different scenarios. However, concerning the first-order configurations, the results for $\beta(r) = \beta_2$ can be obtained directly from those for $\beta(r) = \beta_1$ via the redefinitions $\alpha \rightarrow 2\alpha$ and $h \rightarrow h/4$, from which it is possible to conclude that there is only one effective scenario.

We look for the first-order differential equations by proceeding the minimization of the energy according the Bogomol'nyi prescription, the starting-point being the energy-momentum tensor itself, i.e.

$$T_{\lambda\rho} = 2 (P_{ab} D_\lambda \phi_b)^* P_{ac} D_\rho \phi_c - \eta_{\lambda\rho} \mathcal{L}_{ntop}, \quad (17)$$

where

$$\mathcal{L}_{ntop} = (P_{ab} D_\mu \phi_b)^* P_{ac} D^\mu \phi_c - V(|\phi|) \quad (18)$$

stands for the nontopological sector of the original Lagrange density (1).

The radially symmetric expression for the energy-density coming from (17) reads

$$\varepsilon(r) = \frac{\kappa^2 B^2}{g^2 h W} + h \left[\left(\frac{d\alpha}{dr}\right)^2 + \frac{W}{r^2} \left(\frac{A}{2} - m\right)^2 \right] + V, \quad (19)$$

where we have used the Gauss law (6),

$$A^0 = -\frac{2\kappa B}{g^2 h W} \quad (20)$$

in order to rewrite the contribution coming from A_0 in terms of the magnetic field B . Here, we have also introduced the auxiliary function

$$W(\alpha, \beta) = (1 - \sin^2 \alpha \cos^2(2\beta)) \sin^2 \alpha. \quad (21)$$

It is important to emphasize that, once the function β is assumed to be a constant (according the values appearing in the Eq. (16)), the potential V therefore depends on the field α only, i.e. $V = V(\alpha)$.

We also highlight that that the developments we introduce from now on effectively describe the particular scenario defined by the choices which we have specified in the previous paragraphs, the solutions for $\beta(r)$ being necessarily one of those in (16).

III. THE SOLUTIONS

A. The BPS formalism for $\beta(r) = \beta_1$

In view of the discussion right after the Eq. (16), we proceed a detailed implementation of the first-order BPS formalism for the case

$$\beta(r) = \beta_1 = \frac{\pi}{4} + \frac{\pi}{2}k, \quad (22)$$

from which one gets $\cos^2(2\beta_1) = 0$ and $W(\alpha, \beta_1) = \sin^2 \alpha$. In this case, the total energy provided by the

expression in (19) then reads

$$\begin{aligned}
E &= 2\pi \int_0^\infty \varepsilon(r) r dr \\
&= 2\pi h \int_0^\infty \left[\left(\frac{d\alpha}{dr} \right)^2 + \frac{\sin^2 \alpha}{r^2} \left(\frac{A}{2} - m \right)^2 \right] r dr \\
&\quad + 2\pi \int_0^\infty \left[\frac{\kappa^2 B^2}{g^2 h \sin^2 \alpha} + V \right] r dr, \tag{23}
\end{aligned}$$

which, after some algebraic manipulations, can be written in the form

$$\begin{aligned}
E &= 2\pi h \int_0^\infty \left[\frac{d\alpha}{dr} \mp \frac{\sin \alpha}{r} \left(\frac{A}{2} - m \right) \right]^2 r dr \\
&\quad + 2\pi \int_0^\infty \left(\frac{\kappa B}{g\sqrt{h} \sin \alpha} \mp \sqrt{V} \right)^2 r dr \\
&\quad \pm 2\pi \int_0^\infty \left[(A - 2m) \frac{h \sin \alpha}{r} \frac{d\alpha}{dr} + B \frac{2\kappa\sqrt{V}}{g\sqrt{h} \sin \alpha} \right] r dr, \tag{24}
\end{aligned}$$

or

$$\begin{aligned}
E &= 2\pi h \int_0^\infty \left[\frac{d\alpha}{dr} \mp \frac{\sin \alpha}{r} \left(\frac{A}{2} - m \right) \right]^2 r dr \\
&\quad + 2\pi \int_0^\infty \left(\frac{\kappa B}{g\sqrt{h} \sin \alpha} \mp \sqrt{V} \right)^2 r dr \\
&\quad \mp 2\pi \int_0^\infty \left[(A - 2m) h \frac{d \cos \alpha}{dr} \right. \\
&\quad \quad \left. + \frac{d(A - 2m)}{dr} \frac{2\kappa\sqrt{V}}{g^2\sqrt{h} \sin \alpha} \right] dr, \tag{25}
\end{aligned}$$

where we have used the expression (10) for the magnetic field in order to write the third row in a convenient form.

Now, in order to complete the implementation of the first-order BPS formalism, we need to transform the integrand in the third row in a total derivative. In this work, we attain such goal by means of the following relation

$$\frac{2\kappa}{g^2\sqrt{h}} \frac{d}{d\alpha} \left(\frac{\sqrt{V}}{\sin \alpha} \right) = h \frac{d}{d\alpha} \cos \alpha, \tag{26}$$

which also provides the functional form of the self-interacting potential engendering first-order configurations, i.e.

$$V(\alpha) = \frac{g^4 h^3}{16\kappa^2} \sin^2(2\alpha), \tag{27}$$

from which the total energy (25) reduces to

$$\begin{aligned}
E &= 2\pi h \int_0^\infty \left[\frac{d\alpha}{dr} \mp \frac{\sin \alpha}{r} \left(\frac{A}{2} - m \right) \right]^2 r dr \\
&\quad + 2\pi \int_0^\infty \left(\frac{\kappa B}{g\sqrt{h} \sin \alpha} \mp \frac{g^2 h^{3/2}}{4\kappa} \sin(2\alpha) \right)^2 r dr \\
&\quad \mp 2\pi h \int_0^\infty \frac{d}{dr} [(A - 2m) \cos \alpha] dr. \tag{28}
\end{aligned}$$

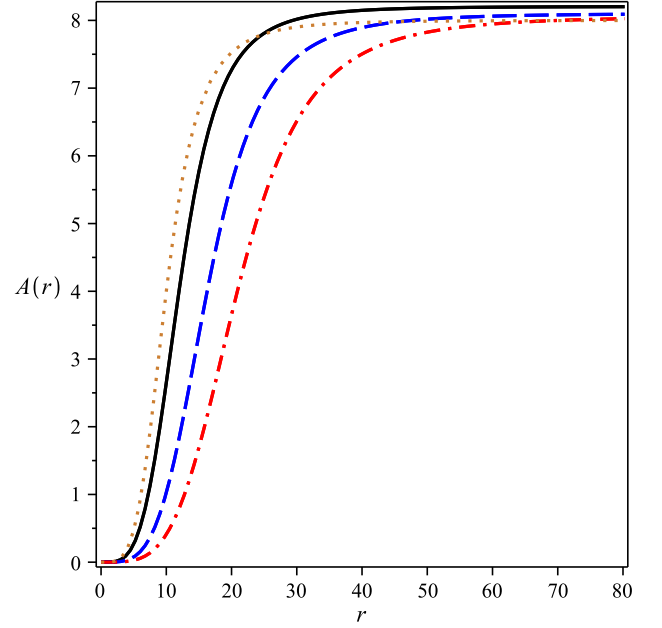


FIG. 2. Numerical solutions to $A(r)$. Conventions as in the Fig. 1. We have also plotted the approximate analytical solution (43). The solutions approach to the value $A_m(r \rightarrow \infty) = 4(m + 1)$, the numerical values being $A_1(r \rightarrow \infty) \approx 8.20526$ for $r_0 = 10$, $A_1(r \rightarrow \infty) \approx 8.10268$ for $r_0 = 15$ and $A_1(r \rightarrow \infty) \approx 8.06025$ for $r_0 = 20$.

It is instructive to point out that the boundary conditions (11) and (12) allow us to calculate the integral appearing in the third row explicitly. In this sense, one gets the energy as

$$\begin{aligned}
E &= E_{bps} + 2\pi h \int_0^\infty \left[\frac{d\alpha}{dr} \mp \frac{\sin \alpha}{r} \left(\frac{A}{2} - m \right) \right]^2 r dr \\
&\quad + 2\pi \int_0^\infty \left(\frac{\kappa B}{g\sqrt{h} \sin \alpha} \mp \frac{g^2 h^{3/2}}{4\kappa} \sin(2\alpha) \right)^2 r dr, \tag{29}
\end{aligned}$$

where

$$E_{bps} = 2\pi \int r \varepsilon_{bps} dr = \mp 2\pi h A_\infty \tag{30}$$

is the lower bound for the energy itself (the Bogomol'nyi bound), the BPS energy density ε_{bps} standing for

$$\varepsilon_{bps} = \mp \frac{h}{r} \frac{d}{dr} [(A - 2m) \cos \alpha]. \tag{31}$$

In such a scenario, the Eq. (29) tells us that the Bogomol'nyi bound is saturated when the profile functions satisfy the first-order differential equations

$$\frac{d\alpha}{dr} = \pm \frac{\sin \alpha}{r} \left(\frac{A}{2} - m \right), \tag{32}$$

$$B = -\frac{1}{gr} \frac{dA}{dr} = \pm \frac{g^3 h^2}{4\kappa^2} \sin \alpha \sin(2\alpha), \tag{33}$$

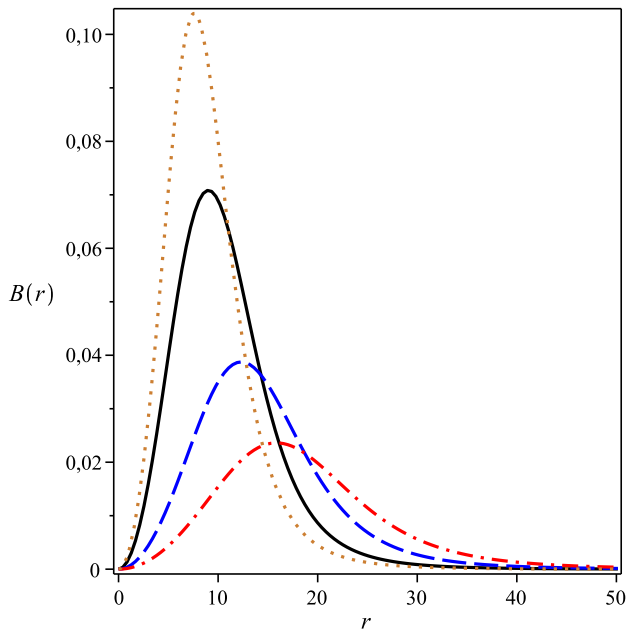


FIG. 3. Numerical solutions to the magnetic field $B(r)$. Conventions as in the Fig. 1. The resulting configurations are rings centered at the origin, their radii being given by (45). In particular, $B_m(r = r_{\max}) \propto r_0^{-2}$, decreasing as r_0 increases.

where the upper (lower) sign holds for negative (positive) values of the vorticity m .

In addition, via the above BPS equations, it is possible to rewrite the corresponding energy density as

$$\varepsilon_{bps} = 2V(\alpha) + 2h \left(\frac{d\alpha}{dr} \right)^2, \quad (34)$$

with $V(\alpha)$ being given by the Eq. (27).

It is interesting to point out that the potential (27) can be written in the form

$$V(|\phi_3|) = \frac{g^4 h}{4k^2} |\phi_3|^2 \left(h - |\phi_3|^2 \right), \quad (35)$$

which spontaneously breaks the original $SU(3)$ symmetry into the $SU(2)$ one, as expected (see the discussion in the beginning of the Section II).

We summarize the overall scenario as follows: once the potential $V(\alpha)$ in (27) was determined, the profile functions $\alpha(r)$ and $A(r)$ can be obtained by solving the differential equations (32) and (33), the resulting radially symmetric configurations possessing the lowest energy possible, i.e. the Bogomol'nyi bound given by the Eq. (30).

It is also worthwhile to point out that, concerning the nontopological configurations we study in this work, the asymptotic contribution appearing in the energy bound (30) will not be necessarily quantized in terms of the winding number m ; this is an essential difference in comparison to the topological case considered in [11].

Beyond the BPS energy, other important quantity to be considered is the flux Φ_B of the magnetic field

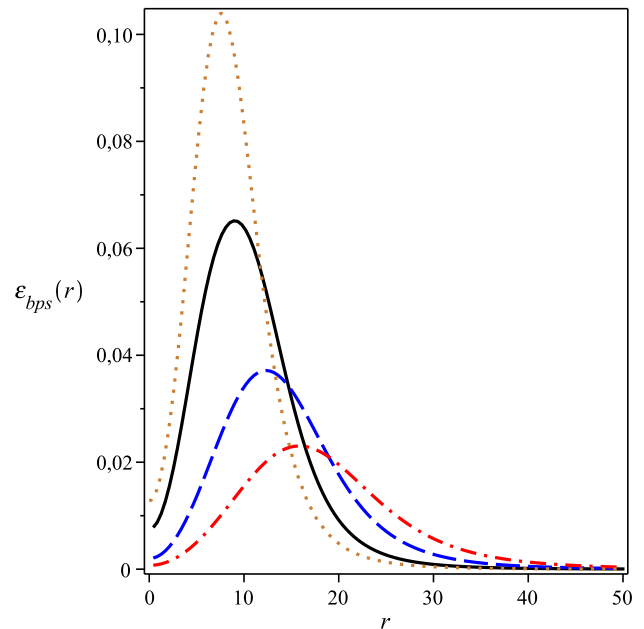


FIG. 4. Numerical solutions to the energy density $\varepsilon_{bps}(r)$. Conventions as in the Fig. 1. Here, $\varepsilon_{bps,m}(r=0) \propto r_0^{-4}$ for $m = 1$ and $\varepsilon_{bps,m}(r=0) = 0$ for $m > 1$.

through the planar space,

$$\Phi_B = 2\pi \int r B(r) dr = -\frac{2\pi}{g} A_\infty, \quad (36)$$

from which one concludes that the energy bound (30) is indeed proportional to the magnetic flux (36), both quantities being not necessarily quantized, as expected for nontopological solitons.

The first-order solutions: the approximate analytical case. It is interesting to point out that, due to the conditions $\alpha(r \rightarrow 0) \rightarrow 0$ and $\alpha(r \rightarrow \infty) \rightarrow 0$, the first-order equations (32) and (33) can be verified to support approximate analytical solutions. In order to calculate them, we suppose that $\alpha(r) \ll 1$ for all r , from which those equations can be approximated, respectively, by

$$\frac{d\alpha}{dr} = \pm \frac{\alpha}{r} \left(\frac{A}{2} - m \right), \quad (37)$$

$$\frac{1}{r} \frac{dA}{dr} = \mp \frac{g^4}{2\kappa^2} h^2 \alpha^2, \quad (38)$$

therefore giving rise to Liouville's equation (here, $\lambda^2 = g^4 h^2 / \kappa^2$)

$$\frac{d^2}{dr^2} \ln \alpha^2 + \frac{1}{r} \frac{d}{dr} \ln \alpha^2 + \frac{\lambda^2}{2} \alpha^2 = 0, \quad (39)$$

its solution standing for

$$\alpha(r) = \frac{4C_1}{\lambda r_0} \frac{\left(\frac{r}{r_0} \right)^{C_1 - 1}}{1 + \left(\frac{r}{r_0} \right)^{2C_1}}, \quad (40)$$

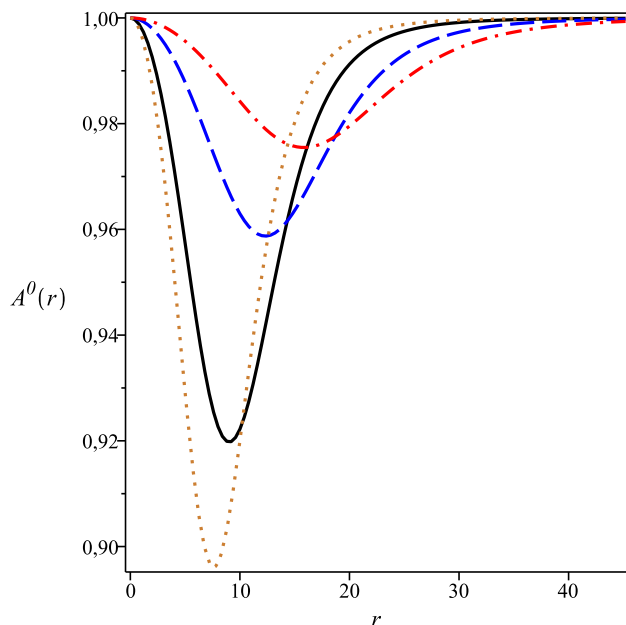


FIG. 5. Numerical solutions to the electric potential $A^0(r)$. Conventions as in the Fig. 1. Here, $A_m^0(r=0) = A_m^0(r \rightarrow \infty) = gh/k$, with $A_m^0(r=r_{\max})$ vanishing for $r_0 \rightarrow \infty$.

where r_0 and C_1 are integration constants. Here, it is worthwhile to highlight that, in order to fulfill the asymptotic condition $\alpha(r \rightarrow \infty) \rightarrow 0$, we must choose $C_1 > 1$.

In addition, given (37) and (40), one gets that the solution to $A(r)$ reads

$$A(r) = 2(m+1 - C_1) + \frac{4C_1 \left(\frac{r}{r_0}\right)^{2C_1}}{1 + \left(\frac{r}{r_0}\right)^{2C_1}}, \quad (41)$$

which satisfies the condition $A(r \rightarrow 0) \rightarrow 0$ for $C_1 = m+1$ only.

The approximate solutions can then be summarized as

$$\alpha_m(r) = \frac{4(m+1)}{\lambda r_0} \frac{\left(\frac{r}{r_0}\right)^m}{1 + \left(\frac{r}{r_0}\right)^{2(m+1)}}, \quad (42)$$

$$A_m(r) = 4(m+1) \frac{\left(\frac{r}{r_0}\right)^{2(m+1)}}{1 + \left(\frac{r}{r_0}\right)^{2(m+1)}}, \quad (43)$$

the last one giving rise to

$$A_{m,\infty} \equiv A_m(r \rightarrow \infty) = 4(m+1), \quad (44)$$

standing for the (approximate) asymptotic condition to be imposed on $A(r)$.

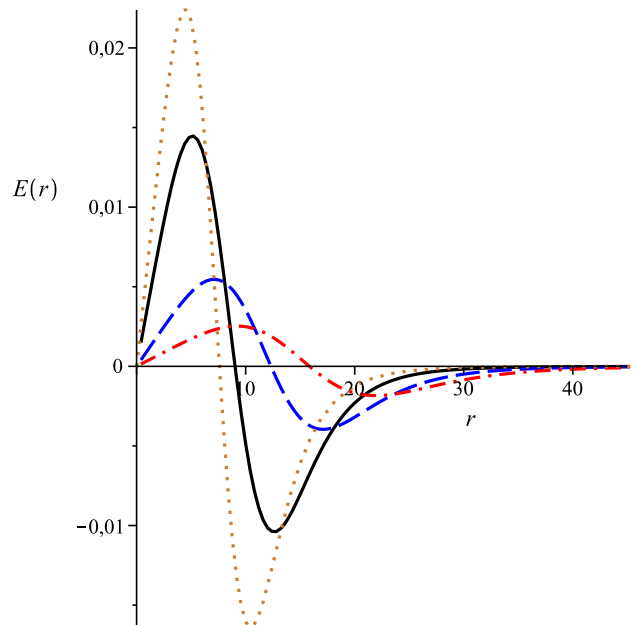


FIG. 6. Numerical solutions to the electric field $E(r)$. Conventions as in the Fig. 1. In this case, $r_{m=1,-} \approx 4.46485$ and $r_{m=1,+} \approx 10.46277$, with $E_{m=1}(r=r_{m=1,-}) \approx 0.02239$ and $E_{m=1}(r=r_{m=1,+}) \approx -0.01636$. Note the inversion of the sign dictating the electric interaction.

It is interesting to note that the approximate solution to $\alpha_m(r)$ stands for a well-defined ring, its radius being given by

$$r_{\max} = r_0 \left(\frac{m}{m+2}\right)^{\frac{1}{2(m+1)}}, \quad (45)$$

(r_{\max} approaching r_0 in the limit $m \rightarrow \infty$), from which one gets

$$\alpha_m(r=r_{\max}) = \frac{2(m+2)}{\lambda r_0} \left(\frac{m}{m+2}\right)^{\frac{m}{2(m+1)}}, \quad (46)$$

i.e. the amplitude of the ring, our previous assumption $\alpha(r) \ll 1$ holding for

$$\lambda r_0 \gg 2(m+2) \left(\frac{m}{m+2}\right)^{\frac{m}{2(m+1)}}, \quad (47)$$

i.e., for a fixed m , there are only a few values to be chosen for λ and r_0 , and vice-versa.

We have also solved the first-order equations (32) and (33) numerically in order to understand the behavior of the profile fields. In this sense, we have obtained the solutions for $m = h = g = \kappa = 1$ and $r_0 = 10$ (solid black line), $r_0 = 15$ (dashed blue line) and $r_0 = 20$ (dash-dotted red line), from which we have plotted the resulting profiles in the figs. 1, 2, 3, 4, 5 and 6 below. We have also depicted the approximate solutions for $m = h = g = \kappa = 1$ and $r_0 = 10$ (dotted orange line), for comparison.

The solutions to the profile function $\alpha(r)$ appear in the Fig. 1. These profiles are well-defined rings centered at

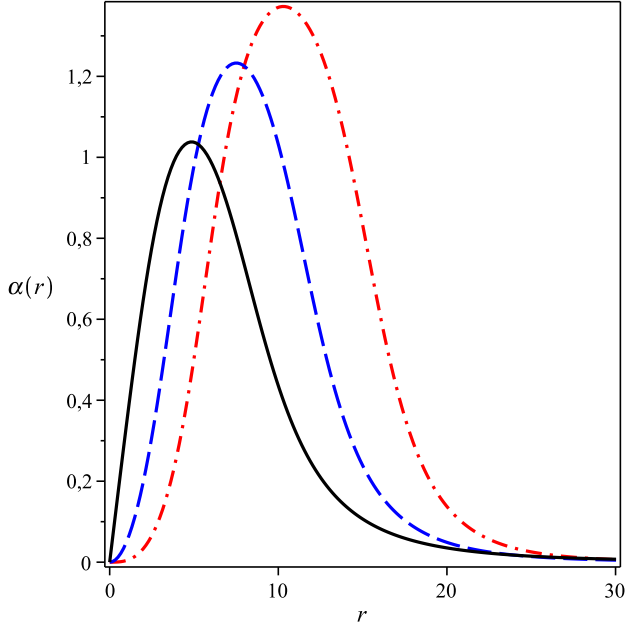


FIG. 7. Numerical solutions to $\alpha(r)$. Here, we have used $h = g = k = r_0 = 1$ and $m = 1$ (solid black line), $m = 2$ (dashed blue line) and $m = 3$ (dash-dotted red line), the resulting scenario being not predictable by any analytical treatment.

the origin, their radii and amplitudes being given, respectively, by (45) and (46), the first (second) one increasing (decreasing) as r_0 itself increases.

The Figure 2 shows the numerical results to the profile function $A(r)$. Here, it is interesting to note the way the solutions try to reach the approximate value $A_m(r \rightarrow \infty) = 4(m+1)$, the true numerical values reading $A_1(r \rightarrow \infty) \approx 8.20526$ for $r_0 = 10$, $A_1(r \rightarrow \infty) \approx 8.10268$ for $r_0 = 15$ and $A_1(r \rightarrow \infty) \approx 8.06025$ for $r_0 = 20$, the overall solutions being monotonic, as expected.

In the Figure 3, we depict the profiles to the magnetic field $B(r)$, the resulting structures also standing for defined rings centered at $r = 0$ (here, both $B(r = 0)$ and $B(r \rightarrow \infty)$ vanish). In particular, the approximate analytical solution to $B_m(r)$ arising from (42) and (43) reads

$$B_m(r) = \pm \frac{g^3 h^2}{2\kappa^2} \alpha_m^2, \quad (48)$$

via which one concludes that the radii of the corresponding rings are also given by (45), the amplitudes being

$$B_m(r = r_{\max}) = \pm \frac{2g^3 h^2 (m+2)^2}{(\lambda r_0)^2 \kappa^2} \left(\frac{m}{m+2} \right)^{\frac{m}{m+1}}, \quad (49)$$

which decrease as r_0 itself increases.

The numerical solutions to the energy density $\varepsilon_{bps}(r)$ are plotted in the Fig. 4. In this case, it is worthwhile to point out that all the solutions fulfill the finite-energy requirement, i.e. $\varepsilon_{bps}(r \rightarrow \infty) \rightarrow 0$, the approximate

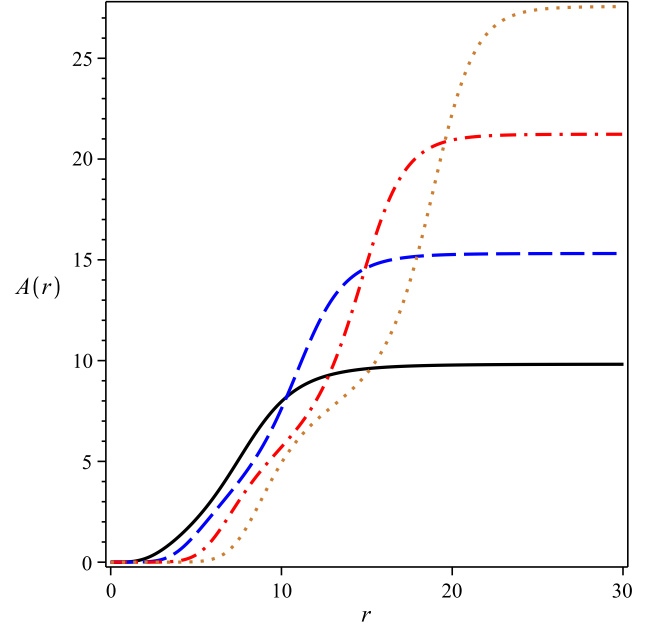


FIG. 8. Numerical solutions to $A(r)$. Conventions as in the Fig. 7, the dotted orange line representing the solution for $m = 4$, the resulting gauge profile presenting an internal structure.

expression for the energy distribution according (34) is

$$\varepsilon_{bps,m}(r) = \frac{g^4 h^3}{2\kappa^2} \alpha_m^2 + 2h \left(\frac{d\alpha_m}{dr} \right)^2, \quad (50)$$

from which we get that the radii inherent to the energy-rings are also defined by the expression in (45). Moreover, we calculate

$$\varepsilon_{bps,m}(r = r_{\max}) = \frac{2h(m+2)^2}{r_0^2} \left(\frac{m}{m+2} \right)^{\frac{m}{m+1}} \quad (51)$$

and

$$\varepsilon_{bps,m}(r = 0) = \begin{cases} \frac{128m^2\kappa^2}{g^4 h r_0^4}, & \text{if } m = 1 \\ 0, & \text{if } m > 1 \end{cases}, \quad (52)$$

with $\varepsilon_{bps,1}(r = 0)$ decreasing as r_0 increases, see the numerical solutions.

We plot the numerical results to the electric potential $A^0(r)$ in the Figure 5, the approximate solution standing for

$$A_m^0(r) = \pm \frac{gh}{\kappa} \left(1 - \frac{1}{2} \alpha_m^2 \right), \quad (53)$$

the resulting profile satisfying $A_m^0(r = 0) = A_m^0(r \rightarrow \infty) = \pm gh/\kappa$, these boundary conditions do not depending on m . Moreover, given (53), one concludes that the corresponding radius is also given by (46), via which we

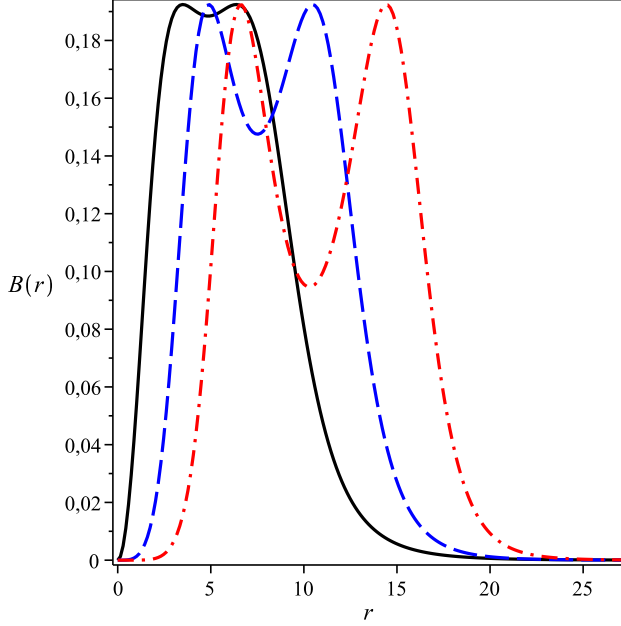


FIG. 9. Numerical solutions to $B(r)$. Conventions as in the Fig. 7. The solution is a double ring centered at the origin, the magnetic field vanishing at the boundaries.

calculate

$$A_m^0(r = r_{\max}) = \pm \frac{gh}{\kappa} \left(1 - \frac{2(m+2)^2}{(\lambda r_0)^2} \left(\frac{m}{m+2} \right)^{\frac{m}{m+1}} \right), \quad (54)$$

which vanishes in the limit $r_0 \rightarrow \infty$. In particular, for $m = h = g = \kappa = 1$ and $r_0 = 10$, one gets that $A_{m=1}^0(r = r_{\max}) \approx 0.89608$, see the Figure 5.

The numerical solutions to the electric field $E(r) = -dA^0/dr$ appear in the Figure 6, the approximate one reading

$$E_m(r) = \frac{gh}{\kappa} \frac{\alpha_m^2}{r} \left(\frac{A_m}{2} - m \right), \quad (55)$$

with $A_m(r)$ itself given by (43). In this case, one gets that

$$\frac{dE_m}{dr} = -\frac{d^2 A_m^0}{dr^2} = \pm \frac{gh}{\kappa} \left[\left(\frac{d\alpha_m}{dr} \right)^2 + \alpha_m \frac{d^2 \alpha_m}{dr^2} \right] \quad (56)$$

vanishes for

$$\left(\frac{d\alpha_m}{dr} \right)^2 = -\alpha_m \frac{d^2 \alpha_m}{dr^2}, \quad (57)$$

whose solutions are

$$r_{m,\mp} = r_0 R_{m,\mp}^{\frac{1}{2(m+1)}}, \quad (58)$$

in which

$$R_{m,\mp} = \frac{a_m \mp b_m}{c_m}, \quad (59)$$

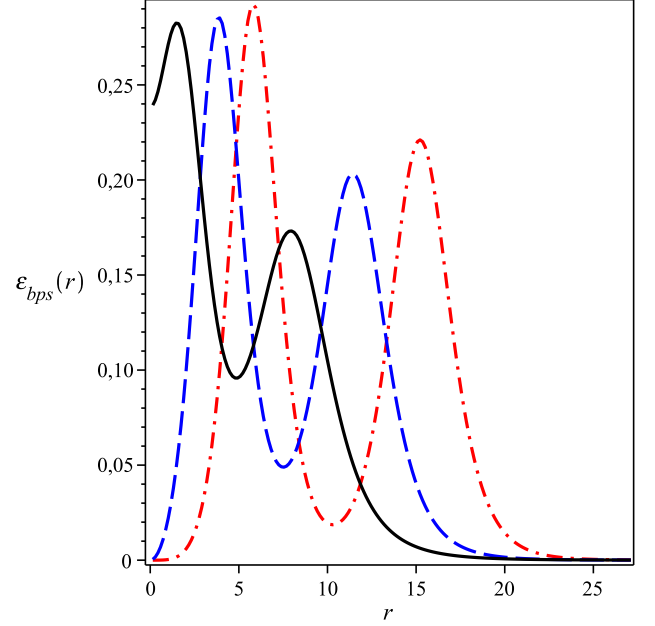


FIG. 10. Numerical solutions to $\varepsilon_{bps}(r)$. Conventions as in the Fig. 7, the energy distribution vanishing at $r = 0$ for $m \neq 1$ only.

the positive coefficients

$$a_m = 4m^2 + 8m + 1, \quad (60)$$

$$b_m = \sqrt{12m^4 + 48m^3 + 61m^2 + 26m + 1}, \quad (61)$$

and

$$c_m = 2m^2 + 9m + 10 \quad (62)$$

depending on the vorticity m explicitly.

In the Figure 6, $r_{m,-}$ and $r_{m,+}$ are the points in which the approximate solution (55) for the electric field reaches its extreme values, i.e.

$$E_m(r = r_{m,\mp}) = \frac{16(m+1)^2 gh}{\lambda^2 \kappa r_0} \Sigma_{m,\mp} \quad (63)$$

for $m > 0$, and

$$E_m(r = r_{m,\mp}) = -\frac{16(m+1)^2 gh}{\lambda^2 \kappa r_0} \Sigma_{m,\mp} \quad (64)$$

for $m < 0$, where

$$\Sigma_{m,\mp} = \frac{R_{\mp}^{\frac{2m-1}{2(m+1)}}}{(1 + R_{\mp})^3} (m - (m+2) R_{\mp}), \quad (65)$$

with both $E_m(r = 0)$ and $E_m(r \rightarrow \infty)$ vanishing. In particular, again for $m = h = g = \kappa = 1$ and $r_0 = 10$, we get that $r_{m=1,-} \approx 4.46485$ and $r_{m=1,+} \approx 10.46277$, with $E_{m=1}(r = r_{m=1,-}) \approx 0.02239$ and $E_{m=1}(r = r_{m=1,+}) \approx$

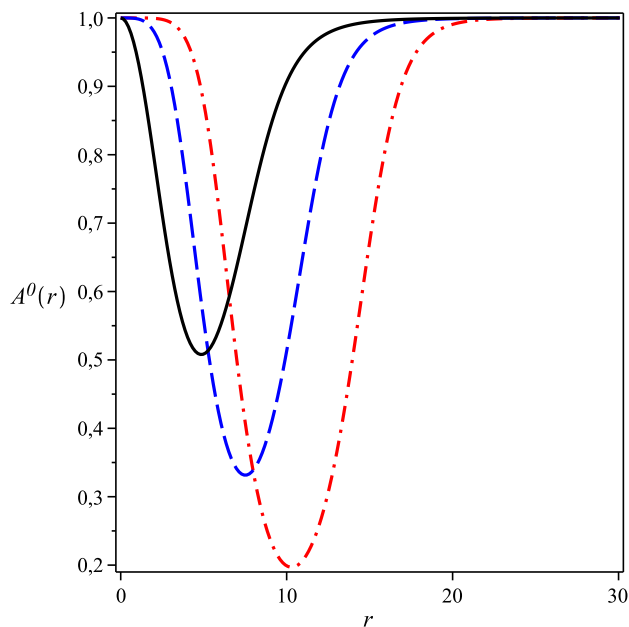


FIG. 11. Numerical solutions to $A^0(r)$. Conventions as in the Fig. 7. This field behaves in the same way as before.

-0.01636 . Here, it is interesting to note the inversion in the sign dictating the electric interaction.

It is instructive to highlight that, in view of the analytical results we have obtained, the energy-bound (30) can be calculated explicitly, its approximate value being given by

$$E_{bps} = \mp 8\pi h(m+1), \quad (66)$$

the magnetic flux (36) standing for

$$\Phi_B = -\frac{8\pi}{g}(m+1), \quad (67)$$

from which one gets $E_{bps} = \pm gh\Phi_B$, the energy of the analytical first-order vortices being then proportional to their magnetic flux, therefore verifying our previous conclusion established right after the Eq. (36). We also point out that both the energy and the magnetic flux of those vortices attained numerically are proportional to the effective values of $A_m(r \rightarrow \infty)$.

The first-order solutions: the full numerical case. It is important to clarify that, beyond the configurations we have presented above, there is a second first-order scenario which can not be predicted by any analytical construction, i.e. it is not possible to approximate its solutions via $\alpha(r) \ll 1$. In order to introduce these new solutions, we again solve the first-order equations (32) and (33) numerically according the conditions (11) and (12), from which we depict the resulting profiles in the figures 7, 8, 9, 10, 11 and 12 below. Here, we use $h = g = \kappa = r_0 = 1$ and $m = 1$ (solid black line), $m = 2$ (dashed blue line) and $m = 3$ (dash-dotted red line).

The new numerical solutions for $\alpha(r)$ are depicted in the Figure 7, the resulting configurations behaving in the

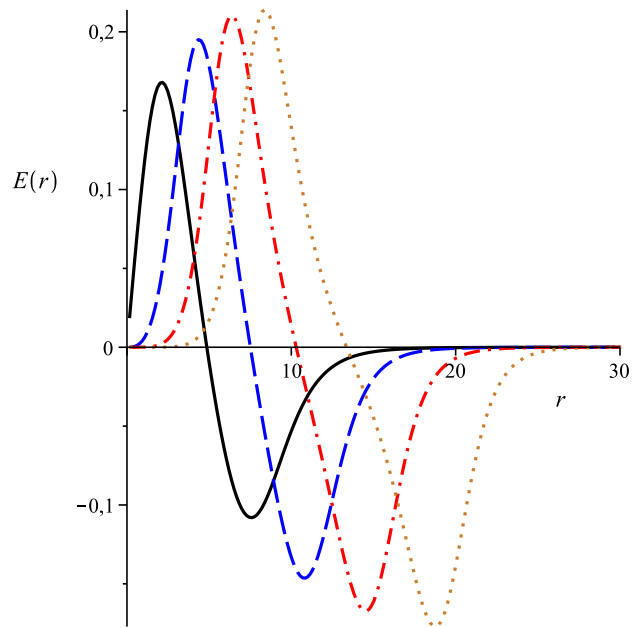


FIG. 12. Numerical solutions to $E(r)$. Conventions as in the Fig. 8. Note the internal structure inherent to the electric field.

same way before, i.e. being rings centered at the origin whose radii and amplitudes increasing as the vorticity m itself increases.

In the Figure 8, we show the profiles to the gauge function $A(r)$, the additional dotted orange line representing the solution for $m = 4$. Here, it is important to point out the existence of an interesting internal structure inherent to the new gauge profiles. Moreover, we emphasize that the new solutions do not obey $A(r \rightarrow \infty) \rightarrow 4(m+1)$, as expected.

The solutions to the magnetic field $B(r)$ and the energy density $\varepsilon_{bps}(r)$ appear in the figures 9 and 10, respectively, both ones standing for double rings centered at $r = 0$. In particular, the magnetic field satisfies $B(r = 0) = 0$ and $B(r \rightarrow \infty) \rightarrow 0$, the energy distribution vanishing at the origin for $m \neq 1$ only, with $\varepsilon_{bps}(r \rightarrow \infty) \rightarrow 0$ (i.e. the finite-energy requirement still holds).

Finally, the figures 11 and 12 show the numerical solutions to the electric potential $A^0(r)$ and the electric field $E(r)$, from which we see that these two fields behave in the same way as those depicted in the figures 5 and 6 (including the sign inversion inherent to the electric field), respectively, the electric one also possessing an internal structure, see the dotted orange line.

B. The BPS formalism for $\beta(r) = \beta_2$

We now summarize the implementation of the BPS formalism for the case

$$\beta(r) = \beta_2 = \frac{\pi}{2}k, \quad (68)$$

which gives $\cos^2(2\beta_2) = 1$ and $W(\alpha, \beta_2) = \frac{1}{4} \sin^2 2\alpha$.

In this case, the total energy obtained from (19) reads

$$E = 2\pi h \int_0^\infty \left[\left(\frac{d\alpha}{dr} \right)^2 + \frac{\sin^2 2\alpha}{4r^2} \left(\frac{A}{2} - m \right)^2 \right] r dr + 2\pi \int_0^\infty \left[\frac{4\kappa^2 B^2}{g^2 h \sin^2 2\alpha} + V \right] r dr. \quad (69)$$

Moreover, after some algebraic manipulation similar to the one we have performed in the case $\beta(r) = \beta_1$, we attain the following condition for the self-interacting potential

$$\frac{4\kappa}{g^2 \sqrt{h}} \frac{d}{d\alpha} \left(\frac{\sqrt{V}}{\sin(2\alpha)} \right) = \frac{h}{4} \frac{d}{d\alpha} \cos(2\alpha), \quad (70)$$

which can be solved to give

$$V(\alpha) = \frac{g^4 h^3}{1024 \kappa^2} \sin^2(4\alpha). \quad (71)$$

In view of this result, the total energy (25) can be written as

$$E = E_{bps} + 2\pi h \int_0^\infty \left[\frac{d\alpha}{dr} \mp \frac{\sin(2\alpha)}{2r} \left(\frac{A}{2} - m \right) \right]^2 r dr + 2\pi \int_0^\infty \left(\frac{2\kappa B}{g\sqrt{h} \sin(2\alpha)} \mp \frac{g^2 h^{3/2}}{32\kappa} \sin(4\alpha) \right)^2 r dr, \quad (72)$$

where the lower-bound now reads

$$E_{bps} = 2\pi \int r \varepsilon_{bps} dr = \mp \pi \frac{h}{2} A_\infty, \quad (73)$$

which is saturated when the profile fields satisfy

$$\frac{d\alpha}{dr} = \pm \frac{\sin(2\alpha)}{2r} \left(\frac{A}{2} - m \right), \quad (74)$$

$$B = \pm \frac{g^3 h^2}{64 \kappa^2} \sin(2\alpha) \sin(4\alpha). \quad (75)$$

We point out that also the potential in (71) can be written as an explicit function of $|\phi_3|$, i.e.

$$V(|\phi_3|) = \frac{g^4}{64 \kappa^2 h} |\phi_3|^2 \left(h - |\phi_3|^2 \right) \left(h - 2|\phi_3|^2 \right)^2, \quad (76)$$

which manifestly breaks the original $SU(3)$ symmetry, as expected.

Here, it is important to highlight that a simple comparison reveals that the first-order results obtained for $\beta(r) = \beta_2$ can be mapped directly from those calculated for $\beta(r) = \beta_1$ via the redefinitions $\alpha \rightarrow 2\alpha$ and $h \rightarrow h/4$.

IV. FINAL COMMENTS

In this work, we have considered the nontopological first-order solitons inherent to a planar gauged $CP(2)$ scenario endowed by the Chern-Simons action, focusing our attention on those time-independent profiles possessing radial symmetry. We have proceeded the minimization of the corresponding energy (the starting-point being the energy-momentum tensor), from which we have established the corresponding first-order framework (a set of two coupled first-order equations and a well-defined lower bound for the total energy itself) inherent to the effective radially symmetric scenario.

In the sequel, we have solved the first-order equations numerically by means of a finite-difference method. In this sense, despite the high nonlinearity, we have identified a special kind of configurations that can be described by approximate analytical solutions in the regimen $\alpha(r) \ll 1$ for all r . The resulting profiles have been depicted and we have commented their main characteristics, from which we have noted an interesting inversion of the sign dictating the electric interaction and the existence of an internal structure inherent to the gauge function.

An interesting issue for a future work includes the search for a more general implementation of the first-order BPS formalism independent of an specific Ansatz. This idea is currently being under investigation and we hope positive results to be presented in an incoming contribution.

ACKNOWLEDGMENTS

This work was supported by the CNPq, CAPES and FAPEMA (Brazilian agencies). In particular, RC thanks the support from the grants CNPq/306385/2015-5, FAPEMA/Universal-00782/15 and FAPEMA/Universal-01131/17, MLD acknowledges the full support from CAPES (postgraduate scholarship), and EH thanks the support from the grants CNPq/307545/2016-4 and CNPq/449855/2014-7.

-
- [1] N. Manton and P. Sutcliffe, *Topological Solitons* (Cambridge University Press, Cambridge, England, 2004).
 [2] E. Bogomol'nyi, Sov. J. Nucl. Phys. **24**, 449 (1976). M. Prasad and C. Sommerfield, Phys. Rev. Lett. **35**, 760 (1975).

- [3] H. B. Nielsen and P. Olesen, Nucl. Phys. B **61**, 45 (1973).
 [4] R. Jackiw and E. J. Weinberg, Phys. Rev. Lett. **64**, 2234 (1990). R. Jackiw, K. Lee and E. J. Weinberg, Phys. Rev. D **42**, 3488 (1990).
 [5] D. Bazeia, E. da Hora, C. dos Santos and R. Menezes,

- Phys. Rev. D **81**, 125014 (2010); Eur. Phys. J. C **71**, 1833 (2011). D. Bazeia, R. Casana, M. M. Ferreira Jr. and E. da Hora, Europhys. Lett. **109**, 21001 (2015). R. Casana, E. da Hora, D. Rubiera-Garcia and C. dos Santos, Eur. Phys. J. C **75**, 380 (2015). R. Casana, M. M. Ferreira Jr., E. da Hora and C. Miller, Phys. Lett. B **718**, 620 (2012). R. Casana, M. M. Ferreira Jr., E. da Hora and A. B. F. Neves, Eur. Phys. J. C **74**, 3064 (2014). R. Casana and G. Lazar, Phys. Rev. D **90**, 065007 (2014). R. Casana, C. F. Farias and M. M. Ferreira Jr., Phys. Rev. D **92**, 125024 (2015). R. Casana, C. F. Farias, M. M. Ferreira Jr. and G. Lazar, Phys. Rev. D **94**, 065036 (2016). L. Sourrouille, Phys. Rev. D **87**, 067701 (2013). R. Casana and L. Sourrouille, Mod. Phys. Lett. A **29**, 1450124 (2014).
- [6] C. Armendariz-Picon, T. Damour and V. Mukhanov, Phys. Lett. B **458**, 209 (1999). V. Mukhanov and A. Vikman, J. Cosmol. Astropart. Phys. **02**, 004 (2005). A. Sen, J. High Energy Phys. **07**, 065 (2002). C. Armendariz-Picon and E. A. Lim, J. Cosmol. Astropart. Phys. **08**, 007 (2005). J. Garriga and V. Mukhanov, Phys. Lett. B **458**, 219 (1999). R. J. Scherrer, Phys. Rev. Lett. **93**, 011301 (2004). A. D. Rendall, Class. Quantum Grav. **23**, 1557 (2006).
- [7] A. D’Adda, M. Luscher and P. D. Vecchia, Nucl. Phys. B **146**, 63 (1978). E. Witten, Nucl. Phys. B **149**, 285 (1979). A. M. Polyakov, Phys. Lett. B **59**, 79 (1975). M. Shifman and A. Yung, Rev. Mod. Phys. **79**, 1139 (2007).
- [8] A. Yu. Loginov, Phys. Rev. D **93**, 065009 (2016).
- [9] R. Casana, M. L. Dias and E. da Hora, Phys. Lett. B **768**, 254 (2017).
- [10] R. Casana, M. L. Dias and E. da Hora, Phys. Rev. D **96**, 076013 (2017).
- [11] V. Almeida, R. Casana and E. da Hora, Phys. Rev. D **97**, 016013 (2018).